water

MDPI

Article

Monitoring Surface Water Area Changes in the Aral Sea Basin Using the Google Earth Engine Cloud Platform

Shuangyan Huang [1,2,3,4,5,6], Xi Chen [1,2,3,5,6,*], Xiaoting Ma [1,3], Hui Fang [1,2], Tie Liu [1,2,3,5,6], Alishir Kurban [1,2,3,5,6], Jianan Guo [1,2], Philippe De Maeyer [4,5,6] and Tim Van de Voorde [4,5,6]

1 State Key Laboratory of Desert and Oasis Ecology, Xinjiang Institute of Ecology and Geography, Chinese Academy of Sciences, Urumqi 830011, China; huangshuangyan15@mails.ucas.ac.cn (S.H.)
2 Research Center for Ecology and Environment of Central Asia, Chinese Academy of Sciences, Urumqi 830011, China
3 University of Chinese Academy of Sciences, Beijing 100049, China
4 Department of Geography, Ghent University, 9000 Ghent, Belgium
5 Sino-Belgian Joint Laboratory of Geo-Information, Urumqi 830011, China
6 Sino-Belgian Joint Laboratory of Geo-Information, 9000 Ghent, Belgium
* Correspondence: chenxi@ms.xjb.ac.cn

Abstract: The surface water area and types in the Aral Sea Basin (ASB) have undergone extensive changes due to the impacts of climate change and anthropogenic activities. This study explores the changes in the surface water area in the ASB based on the Google Earth Engine cloud platform. Then, we integrate multi-source data to identify 1559 lakes and 196 reservoirs from the Joint Research Centre Global Surface Water (JRC GSW) dataset. Our results indicate that the lake area (34,999.61 km^2) is about 10 times that of the reservoir area (3879.08 km^2) in the ASB. The total area of surface water in the ASB decreased by 23,194.35 km^2 or 34.58% from 1992 to 2020. Specifically, the areas of permanent water shrunk at a rate of 1278.6 km^2/year, while the areas of seasonal water increased at a rate of 522.5 km^2/year. The proportion of lakes and reservoirs in the total surface water has decreased from 79.33% (during 1992–2000) to 75.21% (during 2000–2010) to 63.94% (during 2010–2020). The water that should have flowed into the Aral Sea to maintain its permanent water may have been converted into two parts. Part of it might continue to be permanent water but show up in other regions, while part of it might convert to seasonal water (especially in the Aral Sea itself and the ASB plain area). Our study bridges the limitations of previous studies that have ignored seasonal water change and builds a water area list for 1755 lakes/reservoirs ($\geq$0.1 km^2) for the first time. The results can serve as important knowledge for water resource management and sustainable river basin development in ASB.

Keywords: lakes and reservoirs; surface water area; permanent and seasonal; Aral Sea Basin; Google Earth Engine

Citation: Huang, S.; Chen, X.; Ma, X.; Fang, H.; Liu, T.; Kurban, A.; Guo, J.; De Maeyer, P.; Van de Voorde, T. Monitoring Surface Water Area Changes in the Aral Sea Basin Using the Google Earth Engine Cloud Platform. *Water* **2023**, *15*, 1729. https://doi.org/10.3390/w15091729

Academic Editors: Cesar Andrade and Achim A. Beylich

Received: 29 March 2023
Revised: 24 April 2023
Accepted: 27 April 2023
Published: 29 April 2023

1. Introduction

Surface water is a critical component of the hydrological and biogeochemical cycles [1], providing a wide range of ecosystem and social functions, including climate regulation, ecosystem balance, biodiversity protection, freshwater supply, flow regulation, irrigation, and power generation [2,3]. The Aral Sea Basin (ASB) is a vulnerable ecological zone in arid Central Asia. Over the past decades, surface water in the ASB, especially the lakes and reservoirs, has undergone noticeable changes due to natural variability, climate change, increasing water demand, and man-made interventions [4]. The most representative of these changes is the shrinking of the Aral Sea from the fourth-largest lake in the world to one-tenth of its original size, triggering an environmental disaster that threatens regional water security and stability [5]. Therefore, monitoring and understanding the spatiotemporal change of surface water resources in the ASB are essential for ensuring water security, sustaining ecosystem balance, and enhancing human wellbeing [6].

Conventional monitoring approaches that quantify surface water dynamics typically rely on field surveys and statistical extrapolation, which have limited spatial coverage and accuracy [3]. Rigorous field-based surveys of lakes and reservoirs at a fine frequency on a regional scale are still lacking, particularly in remote and inhospitable areas [7,8]. With the development of technology, remote sensing has been proven to be a useful tool for monitoring long-term changes in surface water bodies at a level previously impossible [9–11]. Earth Observation offers a resource- and cost-efficient alternative by providing long-term and large-scale products for monitoring water cycles [12]. Over the past few decades, various surface water datasets have been generated, and the majority of the datasets can be grouped into three categories [13]: (i) Descriptive inventories provide attribute information with a list or point features rather than shoreline polygons. They tend to focus on some representative lakes and reservoirs at a regional scale or global scale and document extensive characterizations, such as waterbody morphometry features, the catchments to which they belong, management information, and geographic distribution [14]. The location is either all indicated by geographic coordinate information (i.e., longitude and latitude) [15,16], partially indicated [17], or not indicated at all [18]. (ii) Object-level databases, often derived from various source maps, provide static polygons of global hydrography with various attributes [13,19].

For example, the global HydroLAKES database documents the shoreline vectors for each of the 1.4 million lakes, with attributes including lake area, water volume, average depth, and shoreline length [19]. Although this object-level database provides detailed knowledge about the geo-referencing information and waterbody morphometry for an individual polygon for each of the lakes and reservoirs, it gives no indication of the temporal changes in water bodies [20]. (iii) Pixel-level datasets provide time-series raster maps of surface water bodies, usually constructed from multi-temporal remote sensing images [4]. For example, the Joint Research Centre Global Surface Water (JRC GSW) dataset [21] documents the location and temporal distribution of surface waters from 1984 to 2020 at 30 m resolution based on the Landsat satellite images, and many studies have made attempts to monitor the surface water changes using the JRC GSW dataset [22,23]. In addition, some land cover/use (LCLU) data also document the interannual variations in surface water bodies, such as the European Space Agency's Climate Change Initiative Land Cover (ESA-CCI-LC) product [24] and the MODIS Land Cover Dynamics product [25]. While pixel-level datasets comprehensively describe the water area dynamics at the pixel level [26,27], they do not provide individual polygons for specific surface water bodies [20]. In summary, although the aforementioned three types of datasets present an opportunity to implement global surface water monitoring, they still provide an incomplete view of surface water. Therefore, datasets that describe the time-series characteristics and discretize each of the water bodies are still needed to better understand the dynamics of surface water and its possible driving forces.

Lakes and reservoirs are regarded as dynamic surface water bodies, with their location and surface extents both affected by climate and human activity [20,21]. In the arid Central Asia region, thousands of small lakes are scattered over the irrigated area of the ASB [28], and they can experience strong intra- and interannual variations (i.e., seasonal and permanent) due to the vulnerability of the region to human activity and climate fluctuations. Recently, a study has suggested that nearly 54.367% of the surface water in Central Asia is at risk of receding and drying up [29]. Previous studies have made attempts to monitor lake area variations of inland water bodies of the ASB or Central Asia. For example, some studies have investigated changes in water bodies using Landsat images or the JRC GSW dataset during some specified years. However, such epoch-based studies might ignore seasonal changes. Other studies map the long-term surface water dynamics based on high temporal resolution but low spatial resolution sensors, such as AVHRR (1 km, 1d) and MODIS (500/250 m, 1d) [30,31], which are not sensitive enough to detect small variations in small water bodies. Additionally, to our knowledge, previous studies have tended to focus only on specific important inland water bodies [31], hotspots of irrigation (e.g., Northwest Uzbekistan) [28], or mountain regions (e.g., the headwaters of the Syr Darya) [32].

Due to the difficulty of acquiring time-series images at a large scale and the complexity of processing images, only a few studies have roughly explored water area changes for Central Asia as a whole [31,33]. The overall basin-scale changes for the ASB and their sub-basin differences are still unknown. With the advent of high-performance computing through the Google Earth Engine (GEE) cloud platform [34,35], surface water can be evaluated across the basin scale at a fine resolution considering both the temporal and spatial dimensions. For example, Wang et al. produced detailed and accurate maps of China's surface water bodies, lakes, reservoirs, and large dams based on the GEE and Google Earth Pro [36]. Therefore, to overcome the aforementioned challenges, this study aims to: (1) identify and map each of the lakes and reservoirs from the JRC GSW dataset and build a water area list for 1755 lakes and reservoirs in ASB; (2) investigate the spatiotemporal patterns of surface water changes, especially the lakes and reservoirs, in ASB during 1992–2020 based on the GEE cloud platform; (3) explore the long-term dynamics of different surface water body types (permanent and seasonal) in ASB. Our results can serve as an important source of information for future water resource management and sustainable river basin development.

2. Materials and Methods

2.1. Study Area

The ASB is located at the crossroads of Europe and Asia and comprises the territory of six states: Uzbekistan, Turkmenistan, Tajikistan, Kazakhstan, Kyrgyzstan, Afghanistan, and Iran (Figure 1a). As an arid and semi-arid region, the ASB exhibits a continental climate, and climate change has accelerated the melting of glaciers in the ASB mountain area over the past decades. Lakes and reservoirs are distributed extremely heterogeneously in the ASB. Specifically, numerous lakes and reservoirs were distributed in the mountain areas and the oasis of the plain area, but few were located in the desert of the plain area. A total of 1559 lakes and 196 reservoirs greater than 0.1 km^2 were investigated in this study (Figure 1a). The ASB is a vast region that mainly includes three parts: the Syr Darya basin, the Amu Darya basin, and the Karakum region (Figure 1b). There are two major transboundary rivers, and the ASB is home to the world's largest man-made canal. The Amu Darya and the Syr Darya originate from the melting snow and glaciers in the eastern mountain area, cross the middle-west plain area, and flow into the Big Aral Sea and Small Aral Sea, respectively. The Karakum Canal, which runs 1375 km and brings 13 km^3 of freshwater annually from the Amu Darya [37], ends up in the Karakum desert and evaporates. According to the Digital Elevation Model (DEM) map (Figure 1c), the ASB can be divided into three main zones: the Aral Sea (Region), ASB plain area, and ASB mountain area (Figure 1d). Specifically, using a mean elevation of 1000 m as the boundary, the eastern and southeastern parts are the ASB mountain area (including the Pamir ranges and Tien Shan ranges), and the western and central parts are the ASB plain area and the Aral Sea (region). To evaluate surface water across the basin scale and subregions (covering upstream, middle stream, and lower stream), this study further divided the ASB into 10 subregions (Figure 1e). The ASB exhibits a continental climate, which is characterized by cold and dry conditions in the mountain area, as well as high temperature and low precipitation in the plain area (Figure 2).

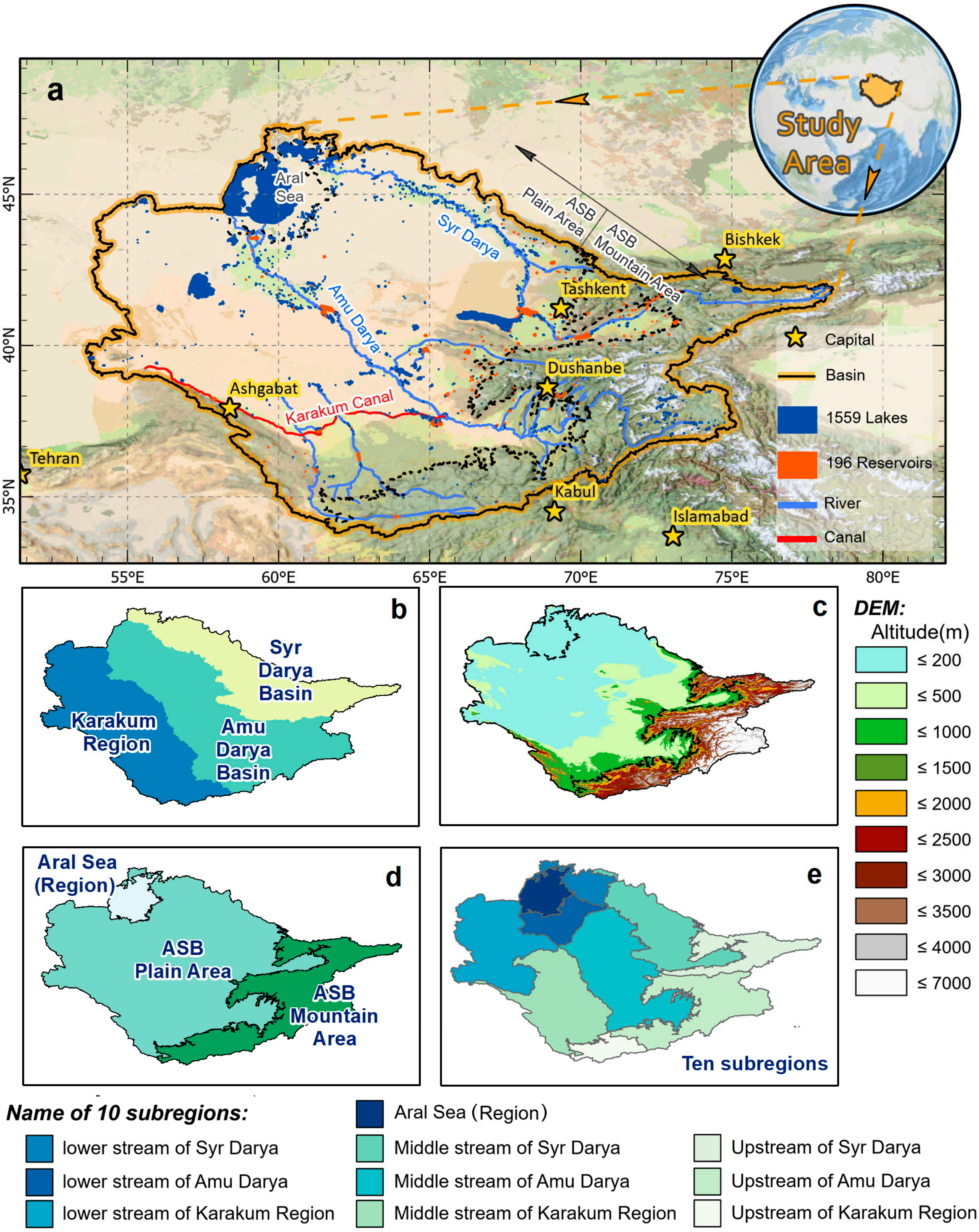

Figure 1. Overview of the study area. (**a**) Location of the ASB. (**b**) The drainage basin boundaries of the three subbasins. (**c**) DEM from the NASA Shuttle Radar Topographic Mission (SRTM). (**d**) Three regions. (**e**) 10 subregions in this study.

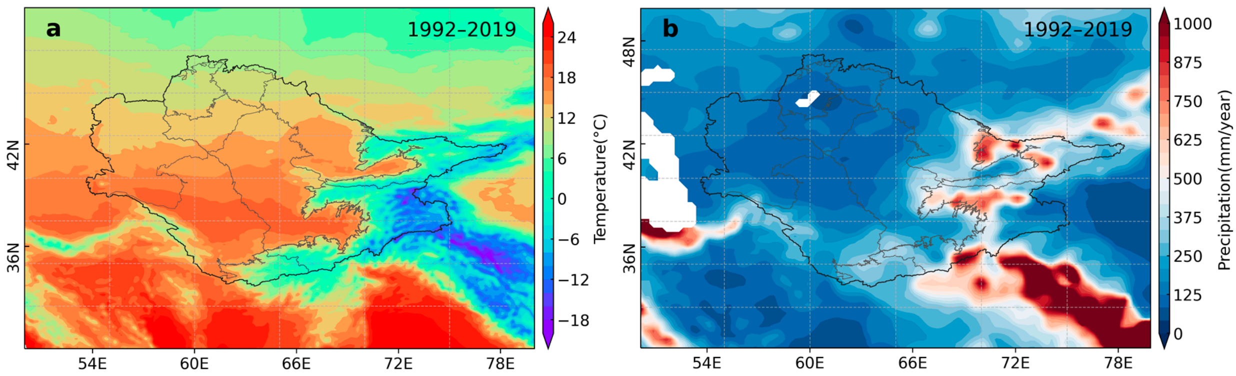

Figure 2. Climate of the ASB. (**a**) Average annual mean temperature during 1992–2019 from ERA5 gridded data. (**b**) Average annual total precipitation during 1992–2019 from GPCC gridded data.

2.2. Data Sources

To map the interannual variations in the surface water area of the ASB, this study used several different types of datasets, including descriptive inventories, object-level databases, and pixel-level datasets. Specifically, the study used the Geo-referenced dams databases, the global HydroLAKES database [19], and the JRC GSW dataset [21].

2.2.1. The Geo-Referenced Dams Databases

The Geo-referenced dams databases were collected from the FAO's Global Information System on Water and Agriculture, which provided detailed information for more than 14,000 dams in each country in the form of Excel files (https://www.fao.org/aquastat/en/databases/dams/, accessed on 5 September 2021). The information of the dams mainly included the name, location (longitude and latitude), dam height, reservoir capacity, reservoir area, and main purpose.

2.2.2. The HydroLAKES Database

The global HydroLAKES database is provided by the World Wildlife Fund and other groups and can be downloaded for free from the website (https://www.hydrosheds.org/products/hydrolakes, accessed on 13 December 2021). HydroLAKES provides consistent and comprehensive shoreline vectors for global surface water bodies through a map generalization method, making it a widely used dataset for global-scale water resource assessments and analyses [38,39]. HydroLAKES was integrated from multiple near-global and regional lake datasets, primarily from the SRTM Water Body Data, supplemented by some regional data from different regions of the world, as well as the Global Lakes and Wetlands Database and Global Reservoir and Dam Database.

2.2.3. The JRC GSW Dataset

The JRC GSW dataset is produced by the European Commission (https://global-surface-water.appspot.com/download, accessed on 23 March 2022) and reveals substantial spatiotemporal changes in global surface water over the last 37 years according to Landsat 5, 7, and 8 images. Due to its good performance and high accuracy, the JRC GSW dataset has been widely used in water resources management, environmental protection, and climate modeling [40,41]. To detect the change in permanent and seasonal water of the ASB, this study collected the following JRC GSW dataset: yearly water history, maximum water extent, transitions, occurrence change intensity, and seasonality.

2.2.4. Other Relevant Data

In addition, the study collected gridded datasets to explore the possible influence factors of the surface water dynamics, including LCLU product from the European Space Agency's Climate Change Initiative (https://www.esa-landcover-cci.org, accessed on 23

October 2021), GPCC monthly precipitation data from the Global Precipitation Climatology Centre (https://opendata.dwd.de/climate_environment/GPCC/html/download_gate.html, accessed on 15 September 2021), and ERA-Land monthly temperature data from the European Centre for Medium-Range Weather Forecasts (https://cds.climate.copernicus.eu, accessed on 22 September 2021). The study also used the SRTM DEM provided by Consortium for Spatial Information (CGIAR-CSI) and the drainage basin outlines from the HydroSHEDS dataset to organize the study area.

2.3. Methods

2.3.1. The Definition of the Permanent Water and Seasonal Water

The JRC GSW dataset provides information on the presence of permanent and seasonal water since 1984 and categorizes each pixel as permanent water, seasonal water, not water, or no observation. If a pixel is covered by water throughout the observation period (typically 12 months), it is classified as permanent water, while a pixel that is not always covered by water is classified as seasonal water. If a pixel is never covered by water during the observation period, it is classified as not water. Pixels that have no observation image available during the entire period are classified as having no observation [21].

2.3.2. Lake and Reservoir Area Extraction

This study used HydroLAKES to acquire the polygons of lakes and reservoirs with areas greater than 0.1 km^2 first. However, HydroLAKES only provide a small amount of information about the reservoirs in the ASB. Therefore, Geo-referenced dams databases and OSM data were further acquired to collect more location information and vectors of the reservoir. For each polygon, we generated a buffer according to its surface area to ensure that the expansion pixel of the isolated surface water bodies falls into the lake detection unit. Then, we used these buffers to further extract the area of permanent water, seasonal water, and their sum for each lake/reservoir from the JRC GSW yearly data. Figure 3 is an example of a lake and reservoir area extraction in the Sarygamysh lake.

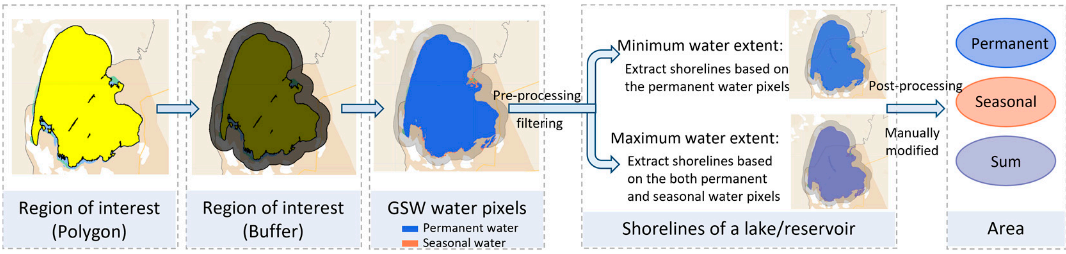

Figure 3. Example of lake and reservoir area extraction. The minimum water extent is the area of the permanent water, while the maximum water extent is the area of the permanent water and seasonal water, i.e., sum.

We established the buffer zone according to one-tenth of the surface area, which not only ensured the dynamic monitoring of the expansion of the lakes/reservoirs but also reduced the amount of data processing and improved the data processing speed. However, there were two exceptions in these 1755 buffers: the Aral Sea and the Sarygamysh lake. The Aral Sea is a sharply shrinking lake, so we used its shoreline from 1980 directly instead of creating a new buffer. On the other hand, the Sarygamysh lake is a sharply expanding lake, so we created a 20 km buffer for it based on the maximum water extent product from the JRC GSW dataset.

2.3.3. Theil–Sen Slope

To analyze the temporal change of regional mean climate datasets (mean temperature, total precipitation), monthly data were used, and time was treated as the dependent variable while the climate data were treated as the independent variable. We estimated the trend of temperature and precipitation for each grid as Equation (1).

$$m_{TS}(y,t) = \underset{i,j\in\{1,\ldots,k\}}{Median}\left\{\frac{y_i - y_j}{t_i - t_j}\right\} \tag{1}$$

where m_{TS} is the Theil–Sen slope; y_i and y_j are data values at time t_i and t_j ($t_i \neq t_j$), respectively; and k is the length of the dataset.

2.3.4. Transition Matrix of the LCLU Maps

For LCLU data, we reclassified them into seven main LCLU types according to the 22 ESA-CCI-LC classes. Then, we computed the transition matrix as Equation (2) to quantify the spatial–temporal pattern of LCLU changes in the ASB from 1992 to 2020. We have

$$T = \begin{bmatrix} A_{11} & A_{12} & \cdots & A_{1j} & \cdots & A_{1n} \\ A_{21} & A_{22} & \cdots & A_{2j} & \cdots & A_{2n} \\ \vdots & \vdots & \ddots & \vdots & \vdots & \vdots \\ A_{i1} & A_{i2} & \cdots & A_{ij} & \cdots & A_{in} \\ \vdots & \vdots & \vdots & \vdots & \ddots & \vdots \\ A_{n1} & A_{n2} & \cdots & A_{nj} & \cdots & A_{nn} \end{bmatrix} \tag{2}$$

where T represents the transition matrix between two maps, A_{ij} demonstrates transition from category i at the beginning to category j at the end of the year, and n is the length of LCLU types ($n = 7$ in this study).

2.3.5. Flowchart of This Study

The flowchart of this study is shown in Figure 4 and consists of three major steps: (1) preliminary mapping of the time-series surface water in the ASB from 1992 to 2020 using the JRC GSW dataset and the GEE platform; (2) further investigation of area changes for 1755 lakes/reservoirs based on the HydroLAKES and JRC GSW dataset; and (3) exploration of spatiotemporal patterns of permanent and seasonal water changes. For more detailed information on each step, please refer to the following sections.

(1) Preliminary Mapping of the Time-Series Surface Water in ASB

In the first step, we generated a time-series map of surface water for the period of 1992–2020 using the yearly water history data from the JRC GSW dataset. The JRC GSW dataset is derived from Landsat satellite images, which provide a spatial resolution of 30 m and a repeat cycle of 16 d, making it suitable for capturing water features. However, due to the large area of the ASB, it is not always possible to obtain cloud-free images covering the entire study area in some years. Additionally, early Landsat data have been plagued by intermittent problems with the data-recording equipment, resulting in missing pixels in some yearly water data. To ensure the accuracy of our analysis, we conducted a manual inspection of the data. We collected the yearly water history data from 1984 to 2020 using the GEE platform and carefully checked for bad data. We removed data from 1984–1988, 1990, 1991, 1995, and 1997, which contained missing pixels. After the manual inspection, we generated a preliminary time-series map of surface water in the ASB from 1992 to 2020, which was of high quality in both spatial and temporal scales.

(2) Further Investigation on the Area Changes of 1755 Lakes/Reservoirs

In the second step, we discretized each of the lakes and reservoirs from the JRC GSW dataset to investigate area changes (detailed method can be found in Section 2.3.2). Manual intervention in this study was necessary for a more reliable result, even though it was a time-consuming and labor-intensive process. Therefore, each of the 1755 buffers underwent visual checking and manual editing based on multiple complementary data sources, including JRC GSW products and Esri world imagery. The main processing steps of the manual check were as follows: removing small islands within the buffers and redundant elements, correcting inappropriate buffers, merging duplicates and overlapping buffers, and solving the topology errors. Surface water occurrence and maximum water extent collected from GEE were used to control the minimum boundaries of the buffers, and high-resolution satellite images accessed from ArcGIS were used to eliminate redundant elements such as small water bodies that connected with rivers or were within wetlands (https://services.arcgisonline.com/ArcGIS/rest/services/World_Imagery/MapServer, accessed on 12 April 2022). The area extent of these elements is extremely unstable, varying greatly with the rise and fall of the river, so they were not considered lake units in this study. Moreover, we deleted rivers or flooded croplands that were mistaken for lakes. Finally, after the manual editing work, we obtained 1755 independent buffers, to each of which we assigned a unique label. We used these buffers to further investigate the area changes of lakes/reservoirs in combination with the yearly surface water data.

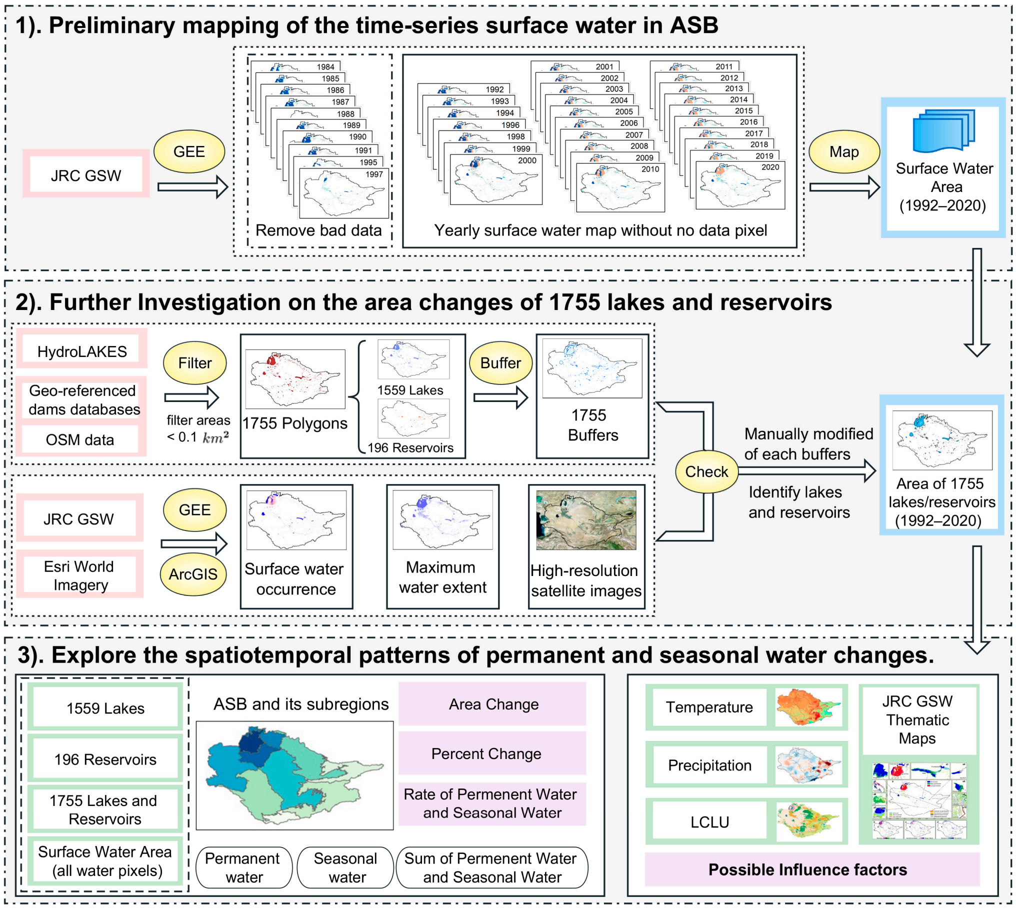

Figure 4. Flowchart of this study. The boxes with a pink border represent the input data of surface water mapping and extraction of the lake/reservoir area changes. The yellow circles indicate the processing methods or platform of the data. The boxes with a blue border indicate the investigation results of this study. The boxes with a light green border indicate the research object of spatiotemporal analysis. The light purple boxes indicate the results of the spatiotemporal analysis.

(3) Explore the spatiotemporal patterns of permanent and seasonal water changes

In the third step, we investigated the long-term dynamics of permanent and seasonal water, which is mainly divided into two parts: Firstly, we investigated the spatiotemporal distribution characteristics of surface water resources by analyzing yearly surface maps produced in the first step. Reservoirs, lakes, lake reservoirs, and surface water (i.e., all water pixels) were selected as the research objects, and their spatiotemporal patterns of permanent and seasonal water changes were explored separately. To conduct a multiscale analysis that covers upstream, middle stream, and lower stream, we further divided our study area into 10 subregions. We compared the differences in area changes between permanent and seasonal water for different subregions and the entire ASB from 1992 to 2020. To analyze the area-change trends of surface water, we adopted a linear regression method. In addition, we calculated the area change and proportion change of permanent water and seasonal water in different regions. Secondly, we examined the temporal changes of the regional climate (mean temperature, total precipitation) and LCLU changes to explore the effects of climate and anthropogenic activity on permanent and seasonal water areas. In addition, we produced a series of thematic maps for the ASB based on the JRC GSW products [21], including (i) transitions in surface water class, (ii) surface water occurrence and occurrence change intensity, and (iii) seasonality.

3. Results

3.1. Spatiotemporal Distribution Change of Surface Water (All Water Pixels)

At the basin and regional scale: Between 1992 and 2020, the areas of various types of surface water bodies, including permanent waters, seasonal waters, and their sum, were identified (Figure 5), which is essential for understanding changes in water resources in ASB and its subregions. At the basin scale, the total surface water area (i.e., sum of the permanent and seasonal water areas) in ASB decreased by 23,194.35 km^2 or 34.58% from 67,075.28 km^2 in 1992 to 43,880.93 km^2 in 2020, with a significant slope of 756.1 km^2/year and R^2 of 0.592 (Figure 5a). The areas of permanent (Figure 5d) and seasonal (Figure 5g) water in ASB showed totally dissimilar patterns during 1992 to 2020, with the former steadily shrinking at a rate of 1278.6 km^2/year, while the latter steadily increased at a rate of 522.5 km^2/year. The decreasing trend of the total surface water areas in the whole ASB (Figure 5a) slowed down from 2000 to 2020 at a rate of 184 km^2/year (not significant at R^2 = 0.066 and p = 0.274), because the areas of permanent (Figure 5d) and seasonal (Figure 5g) water showed a slowed-down decrease trend of 972 km^2/year (significant) and a higher increase trend of 788 km^2/year (significant), respectively. At the regional scale, the total surface water areas in the ASB plain area (Figure 5b) increased by 7772.91 km^2 or 34.92% from 22,260.16 in 1992 to 30,033.07 in 2020, with a significant slope of 312.6 km^2/year during 1992–2020 and 513.8 km^2/year during 2000–2020. Meanwhile, the total surface water areas in the ASB mountain area (Figure 5c) increased by 988.81 km^2 or 89.84% from 1100.67 km^2 in 1992 to 2089.48 km^2 in 2020, with a significant slope of 18.5 km^2/year during 1992–2020 and 24.7 km^2/year during 2000–2020. In addition, we found that permanent water areas (Figure 5e,f) changed at a much slower rate than seasonal ones (Figure 5h,i). In other words, whether in the ASB plain or mountain areas, surface water areas fluctuated more due to seasonal water.

At the subregional scale: Water resources in ASB are concentrated in the Aral Sea and ASB plain area, so changes in water resources in these regions are more dramatic compared to the ASB mountain area. Specifically, area loss of surface waters in ASB occurred mainly in the Aral Sea (Figure 5), resulting in an overall decrease in the total surface area of 31,956.07 km^2 or 73.10% from 43,714.45 km^2 in 1992 to 11,758.38 km^2 in 2020, of which permanent water decreased by 34,317.25 km^2 or 82.13%, while seasonal water increased by 2361.18 km^2 or 122.23%. By contrast, the yearly surface water areas showed a wide increase across the rest of the subregions of the ASB except for the lower Karakum region (Figure 5j).

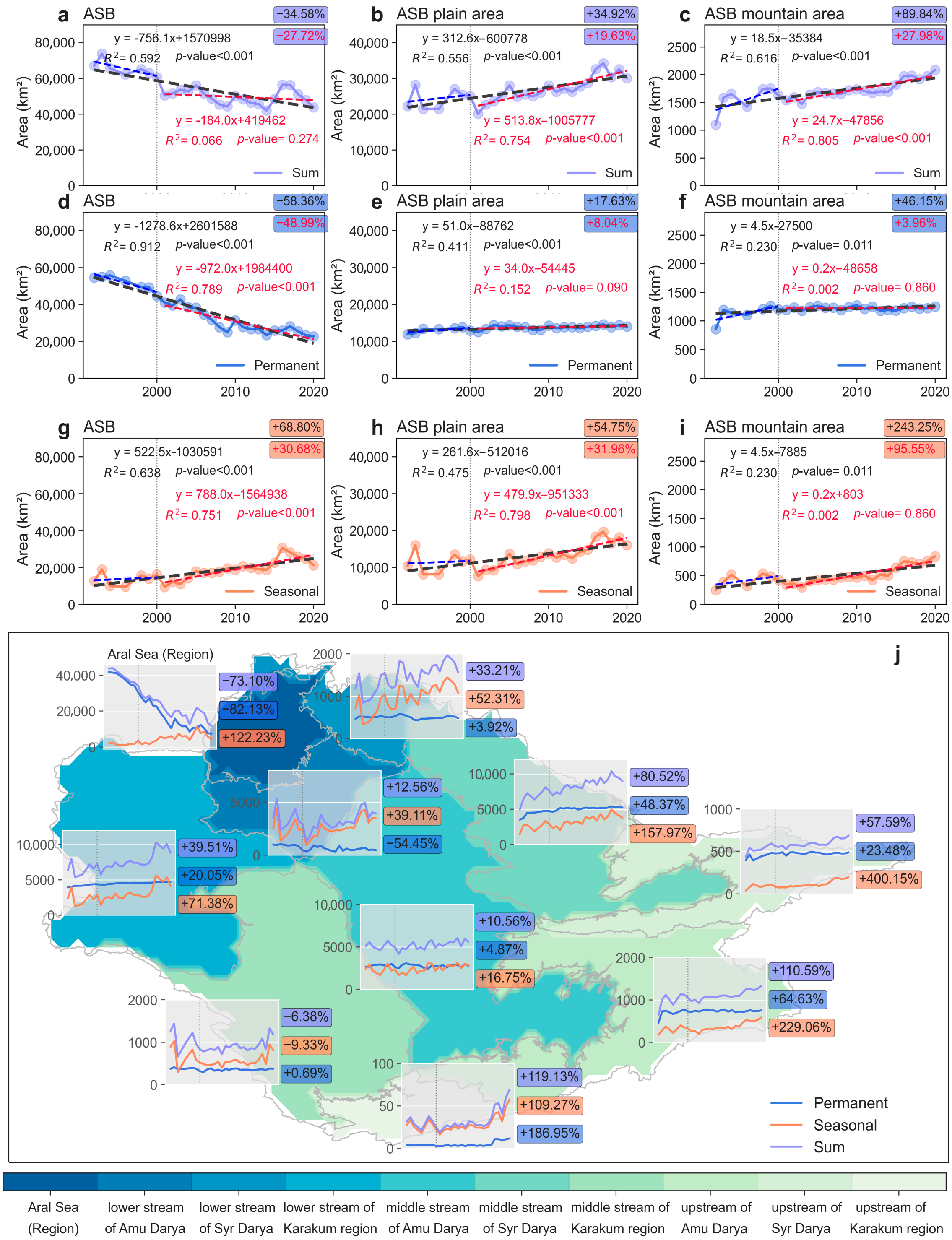

Figure 5. Changes in area of different types of surface water in ASB, ASB plain area, and ASB mountain area between 1992 and 2020. (**a**–**c**), Sum of the permanent and seasonal water areas. (**d**–**f**), Permanent water areas. (**g**–**i**), Seasonal water areas. (**j**) Changes in area of different types of surface water in 10 subregions of the ASB (note the y-axis, which was plotted on the ordinate in km^2). In each panel of this figure, the numbers in the box with different colors represent the percentage change in different types of surface water bodies. The regression lines are marked with black dash lines (1992–2020), blue dash lines (1992–2000), and red dash lines (2000–2020). Changes in area during 1992–2020 are shown by black values, and those during 2000–2020 are shown by red values.

3.2. Changes in Lakes

This study investigated the area change of a total of 1559 lakes ($\geq$0.1 km^2), as shown in Figure 6. At the basin scale, these lakes covered an average total area of 34,999.61 km^2 between 1992 and 2020, with a ratio of permanent water to seasonal water of about 6.9. The multi-year average of the total lake area decreased sharply during the 1992–2000, 2000–2010, and 2010–2020 periods, with the ratio of permanent water to seasonal water fluctuating. The orders were 26.12, 7.79, and 3.17, respectively. The fluctuation was mainly due to the increase of seasonal water while the permanent water decreased. It is worth noting that, although the total lake area of the ASB appears to be relatively high, about 70% is contributed by the Aral Sea. Except for this largest terminal lake in the basin, the other 1558 lakes share only about 30% of the area. With the shrinkage of the Aral Sea, the multi-year average of the total lake area of the ASB decreased from 48,105.55 km^2 during 1992–2000 to 27,247.69 km^2 during 2010–2020. In contrast, the multi-year average of the total lake area of the ASB plain area increased from 9033.16 km^2 during 1992–2000 to 10,155.35 km^2 during 2010–2020. Finally, at the regional scale, the multi-year averages of the total lake area of the ASB plain area and ASB mountain area during 1992–2020 were 9819.44 km^2 and 630.63 km^2, respectively, with the ratios of permanent water to seasonal water of 11.67 and 44.12, respectively. At the subregional scale, the top three regions that possessed the largest lake area from 1992 to 2020 were the Aral Sea (Region), the lower stream of the Karakum Canal Region, and the middle stream of the Syr Darya, with multi-year average total lake areas of 24,549.54 km^2, 4391.69 km^2, and 3552.01 km^2, respectively. In terms of the ratios of permanent water to seasonal water, the top three regions were upstream of the Syr Darya (74.54), upstream of the Amu Darya (30.43), and lower stream of the Karakum Canal Region (27.64). The ratio of permanent water to seasonal water in lakes of the Aral Sea (Region) dropped from 32.54 (1992–2000) to 6.69 (2000–2010) and 1.91 (2010–2020).

3.3. Changes in Reservoirs

In this study, we investigated the area change of a total of 196 reservoirs ($\geq$0.1 km^2), as shown in Figure 7. At the basin scale, these reservoirs covered an average area of 3879.08 km^2 between 1992 and 2020, with a ratio of permanent water to seasonal water of about 1.84. The multi-year average of the total reservoir area decreased sharply during three time periods (1992–2000, 2000–2010, and 2010–2020), with the average total reservoir area being 3776.46 km^2, 3889.27 km^2, and 3950.57 km^2, respectively. For reservoirs, the ratio of permanent water to seasonal water was relatively stable in these periods, with values of 1.91, 1.71, and 1.86, respectively, and the small changes were mainly related to the increase in seasonal water. On the regional scale, most of the reservoirs were found in the ASB plain area rather than the ASB mountain area. The multi-year averages of the total reservoir areas in the ASB plain area and ASB mountain area between 1992 and 2020 were 3408.68 km^2 and 470.40 km^2, respectively, and the ratios of permanent water to seasonal water were 1.65 and 4.75, respectively. On the subregional scale, the top three regions in terms of total reservoir area between 1992 and 2020 were the middle stream of the Syr Darya (1644.45 km^2), the middle stream of the Amu Darya (878.85 km^2), and the middle stream of the Karakum Canal Region (753.06 km^2), respectively. In terms of the ratio of permanent water to seasonal water of the reservoirs, the top three regions were the upstream of the Syr Darya (5.25), the lower stream of the Karakum Canal Region (5.16), and the upstream of the Amu Darya (3.6).

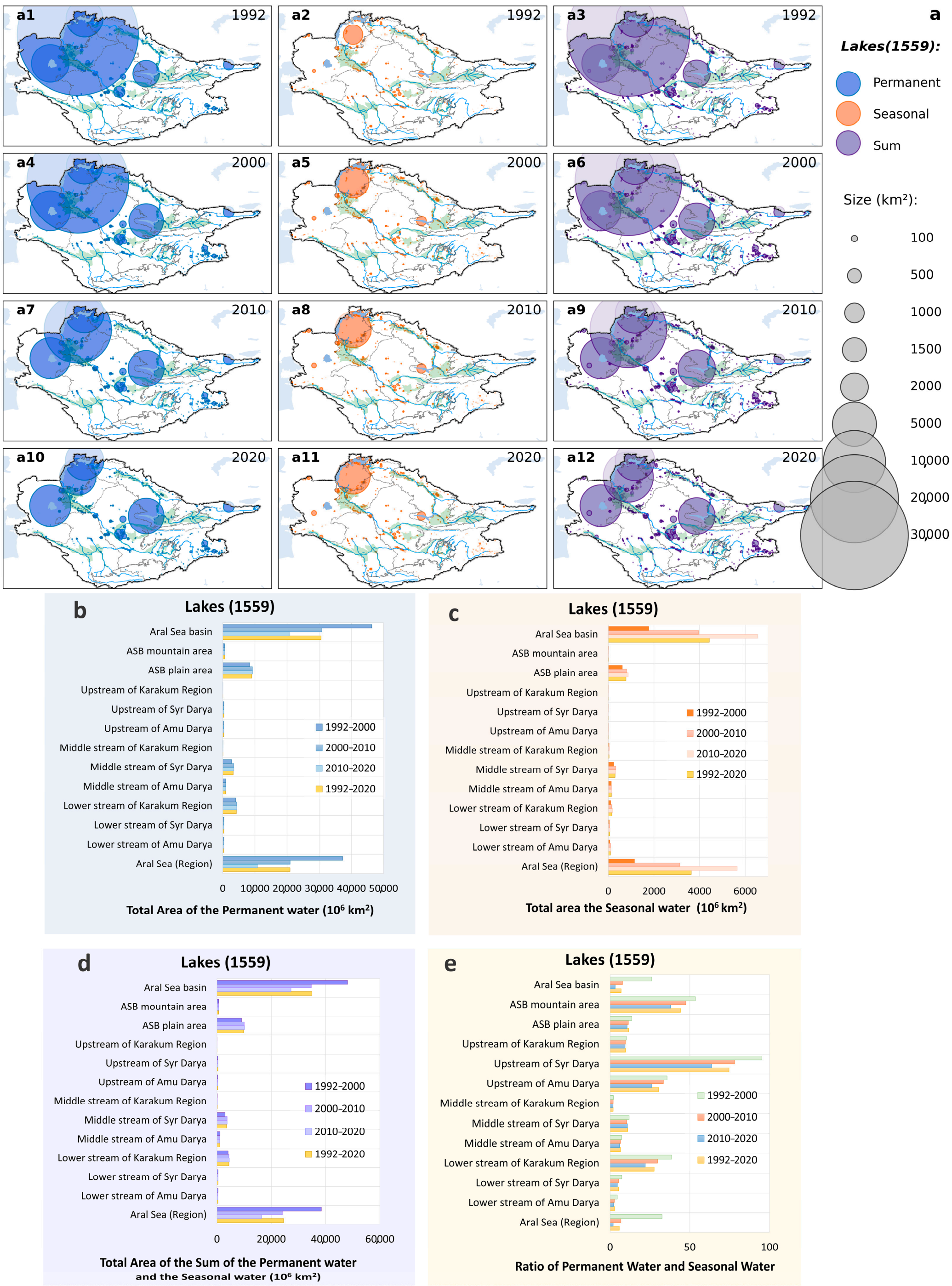

Figure 6. Change analysis of the lakes area in ASB, including the permanent water area, seasonal water area, and their sum. (**a**) Spatiotemporal pattern of 1559 lakes in the particular years (1992, 2000, 2010, and 2020). In each panel of the (**a1**–**a12**), the blue bubbles represent the permanent water area of the lakes, the orange bubbles represent the seasonal water area of the lakes, and the purple bubbles represent the total area of the lakes (i.e., the sum of the permanent and seasonal water area). The size of the bubble is used to show the size of the lake area. (**b**–**d**) Mean annual total area of different water types in different periods for the ASB and its subregions. (**e**) Ratio of permanent water and seasonal water.

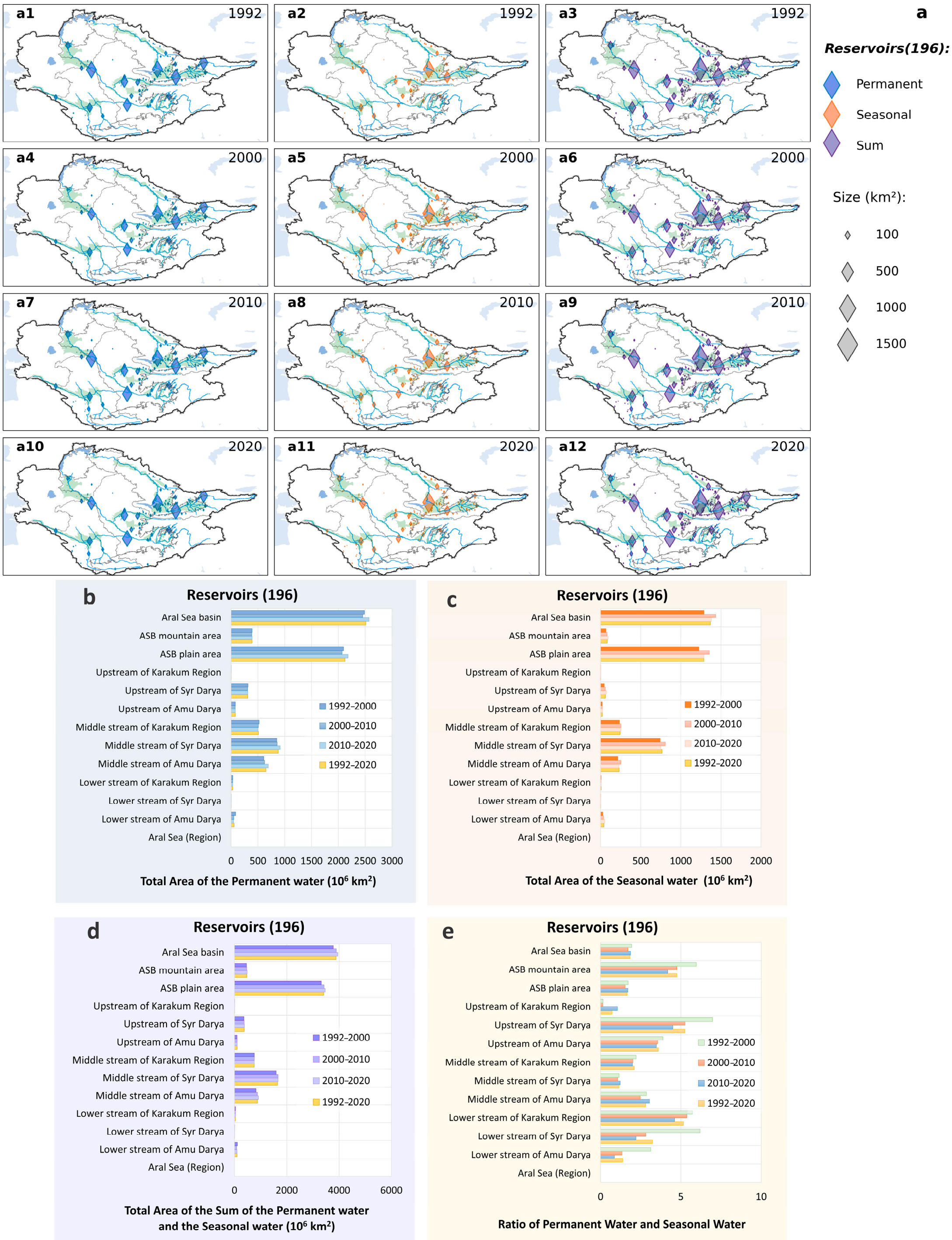

Figure 7. Change analysis of the reservoirs area in ASB, including the permanent water area, seasonal water area, and their sum. (**a**) Spatiotemporal pattern of 196 reservoirs in the particular years (1992, 2000, 2010, and 2020). In each panel of the (**a1**–**a12**), the blue diamonds represent the permanent water area of the reservoirs, the orange diamonds represent the seasonal water area of the reservoirs, and the purple diamonds represent the total area of the reservoirs (i.e., the sum of the permanent and seasonal water area). The size of the diamond is used to show the size of the reservoir area. (**b**–**d**) Mean annual total area of different water types in different periods for the ASB and its subregions. (**e**) Ratio of permanent water and seasonal water.

3.4. Surface Water Structure in ASB

The long-term variations of permanent water and seasonal water were then explored, and the change process is summarized in Figure 8. The results indicate that the structure of water resources in ASB has changed, and the proportion of lakes/reservoirs area in the total surface water area has decreased from 79.33% during 1992–2000 to 75.21% during 2000–2010 and 63.94% during 2010–2020. Overall, the surface water in ASB covered an average area of 53,675.01 km^2 from 1992 to 2020, of which lakes and reservoirs commanded 72.43%. At the regional scale, the proportion of lakes and reservoirs area in the Aral Sea (Region) to the ASB decreased significantly, from 58.82% (during 1992–2000) to 46.88% (during 2000–2010) to 33.71% (during 2010–2020). In contrast, the proportion of lakes and reservoirs areas in the ASB mountain area to the ASB increased slightly, from 1.62% (during 1992–2000) to 2.15% (during 2000–2010) to 2.31% (during 2010–2020). Meanwhile, the proportion of lakes and reservoirs areas in the ASB plain area to the ASB increased significantly, from 18.89% (during 1992–2000) to 26.18% (during 2000–2010) to 27.92% (during 2010–2020). At the subregional scale, the hotspots of increasing lakes/reservoirs area in the ASB plain area were the lower stream of Karakum Region, the middle stream of Syr Darya, and the middle stream of Amu Darya.

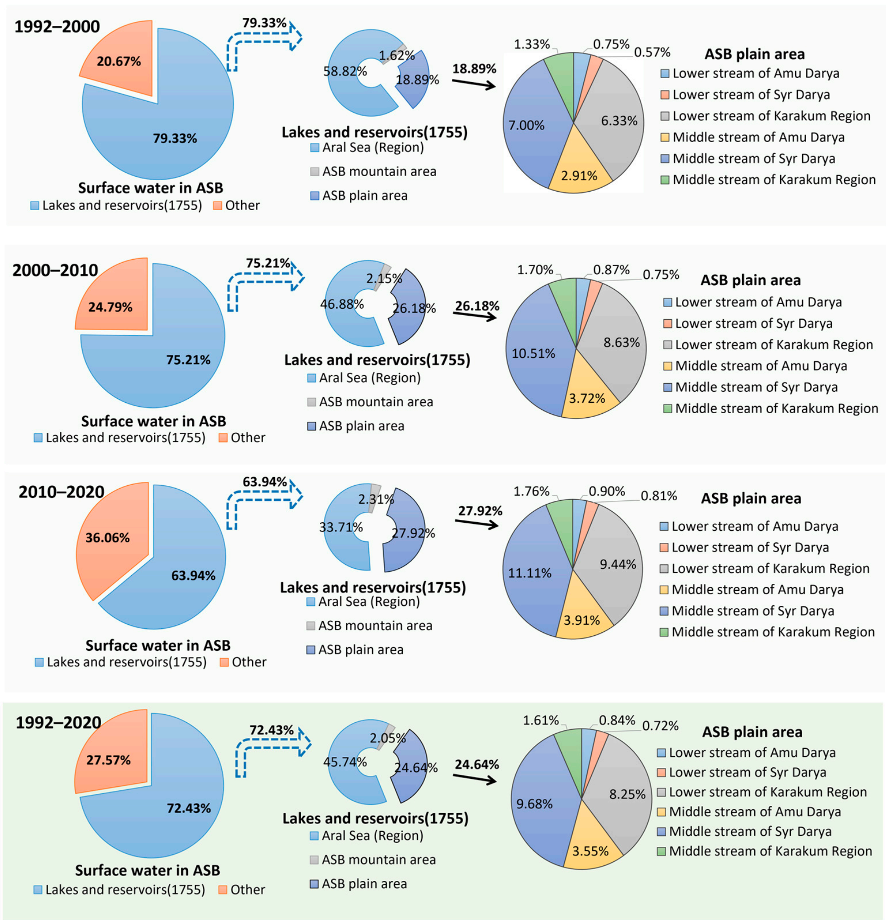

Figure 8. Surface water structure and regional proportion of the ASB, including four time periods: 1992–2000, 2000–2010, 2010–2020, and 1992–2020. The pie chart in the left panel shows the constituent of the total area of surface water in ASB. The pie chart in the middle panel shows the proportion of lake and reservoir areas in the three regions of the ASB to the total area of surface water in ASB. The pie chart in the right panel shows the shows the proportion of lake and reservoir areas in the six subregions of the ASB plain area to the total area of surface water in ASB.

3.5. Climate Change and LCLU Change in ASB

Changes in surface water area and water body types are related to complex climate change and anthropogenic activity. Therefore, we explored the annual average temperature change (Figure 9a), annual total precipitation change (Figure 9b), and land use and land cover change (Figure 9c) in the ASB to explore the possible reasons for surface water changes. As show in Figure 9, the annual mean temperature in the ASB increased significantly from 10.13 °C to 12.23 °C during 1992–2019, while the annual total precipitation increased slightly from 252.61 mm/year to 263.38 mm/year. Figure 9c suggested that the barren area is a major LCLU type in the ASB, occupying about 44.06% of the entire basin in 1992, which had increased 12,338.5 km^2 from 1992 to 2019, followed by grassland (occupying about 20.53%, total decreased 6100.31 km^2), croplands (occupying about 16.89%, slightly increased 807.41 km^2), and woody vegetation (occupying about 12.48%, total increased 1574.31 km^2). Although the urban and built-up areas only occupied about 0.07% of the entire basin in 1992, it gives an overall increase of 6760.11 km^2.

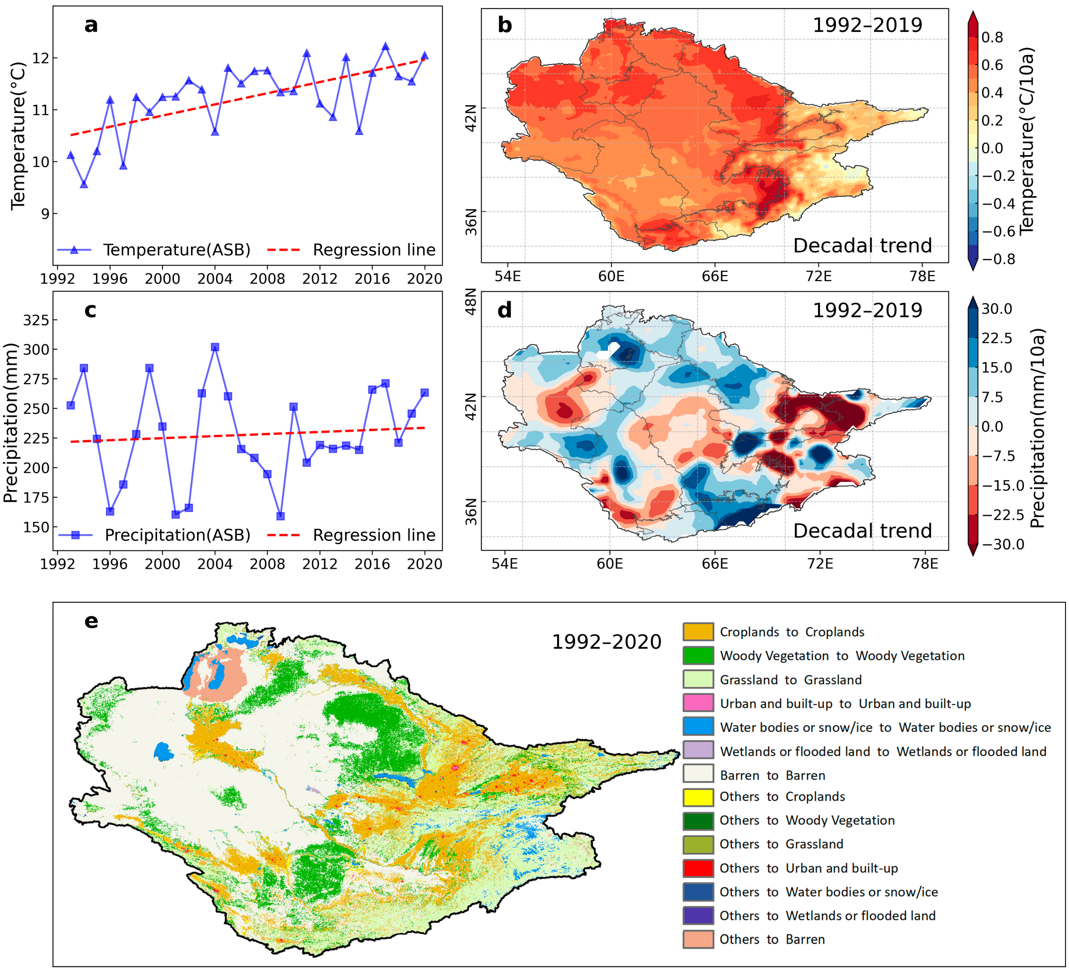

Figure 9. Climate change and LCLU change in ASB. (**a**,**c**) Temporal change in annual mean temperature and annual total precipitation at basin scale. (**b**,**d**) Decadal trends and temporal change in annual mean temperature and annual total precipitation from 1992 to 2019 at pixel scale. (**e**), Geospatial maps of major land cover transitions from 1992 to 2020.

4. Discussion

4.1. Variation Characteristics of Lake and Reservoirs

Surface water in the ASB has undergone significant changes in both water area and water types in the past decades. In this study, we first investigated the area changes of

1755 lakes and reservoirs in the ASB based on the HydroLAKES and JRC GSW dataset. The lake area in the upstream region of the Amu Darya has increased. Previous studies have found that this region has many glaciers [42,43]. Combining Figure 9 with these studies, we found that the temperature in this region has increased while precipitation has decreased from 1992 to 2020. Therefore, we believe that the increased lake area in the upstream of the Amu Darya is related to the eruption of glacial lakes. This speculation is supported by the results of previous studies [44,45].

In addition, the lake area in the lower stream of the Karakum region has also increased significantly, mainly due to the presence of drainage water from the main channel to the lake basin [46]. Reduction of the lake area mainly occurred in the central and western parts of the study area, especially in the middle and lower streams of the Amu Darya and Karakum Canal Region. According to Figure 9, the precipitation in these areas has decreased while the temperature has increased, i.e., in the natural state, the rainfall inflow to the lakes of these regions has decreased, while lake evaporation has been promoted due to the increase in temperature [47,48]. Figure 9c shows that these areas have experienced significant urban expansion in the past 28 years, which means the lakes in these areas are vulnerable to human activities [49].

4.2. Variation Characteristics of Surface Water Area

The present study aimed to map the time-series surface water in ASB and its subregions from 1992 to 2020 using the JRC GSW dataset and the GEE cloud platform. The study results showed that the proportion of permanent water in the surface water of ASB has continued to decline, while the proportion of seasonal water in surface water has continued to increase. The area of permanent water in ASB has decreased sharply, mainly due to the disappearance of permanent water in the Aral Sea and the lower stream of the Amu Darya. In contrast, the seasonal water area in ASB has increased sharply, and the increasing seasonal water comes from all subregions except the middle stream of the Karakum region.

Interestingly, although the permanent water decreased by 54.45% in the lower stream of the Amu Darya, its total amount of surface water increased by 12.56%. This means that the increased water area in the lower stream of the Amu Darya was determined by seasonal water (with a 39.11% increase). These new seasonal waters not only exist in lakes, reservoirs, ponds, rivers, or ditches (a1–a8 in Figure 10) but may also exist in croplands of the irrigated areas (a9–a10 in Figure 10). In addition, there are noticeable new seasonal water bodies in the lower stream of the Amu Darya and middle stream of the Syr Darya. Previous studies [50–52] have shown that unreasonable irrigation practices are common in these areas. For example, to grow cotton under severe saline–alkali stress, farmers often have to leach the fields through flood irrigation in winter [53]. Moreover, much of the irrigation and drainage infrastructure in ASB was built during the Soviet era and is already dilapidated. Furrow irrigation technology is still widely used in ASB, which is less water-efficient than drip irrigation technology [28,50]. These unreasonable irrigation practices have caused an increase in seasonal water bodies in the ASB plain area, and these seasonal waters may be the source of increased evapotranspiration in ASB [54].

4.3. Effects on the Water Balance

Redistribution of surface water in the ASB has not only deprived the freshwater that should have reached the Aral Sea, but also changed the water balance in the basin. For instance, land–water conversion occurring in the ASB is greatly affecting the evaporation processes [55] and has altered the local climate patterns [56], and climate warming will further promote potential evaporation. Previous studies illustrated that the actual evapotranspiration (AET) in the whole ASB has intensified with a 10.13% (+37.62 km^3) increase from 1980 to 2019 [54]. Surface runoff and groundwater recharge are also important parts of water balance, which were also perturbing in the ASB over the past decades [57]. According to the previous studies, the mean annual total river discharge of all rivers in the ASB is around 116 km^3, of which the Amu Darya average annual runoff was roughly 79.4 km^3 and the Syr Darya was roughly 36.6 km^3 [58]. In 2020, the mean annual total river discharge in the basins was only 96.44 km^3 or 83.14% of the mean annual total river discharge [59]. As a terminal lake without flow discharge, the long-term water balance of the Aral Sea is determined by river inflow, precipitation, evaporation, and groundwater intake [5]. After evaporative losses contribute, roughly 55 km^3/year of discharge intake to the Aral Sea [60]. Trend map of the terrestrial water storage (TWS) changes (Figure 11) shows that the Aral Sea (Region) has undergone noticeable water loss from 2003 to 2020. While the southwest of the ASB plain area illustrated an increasing TWS trend, in this region, expand surface water bodies have increased water storage. Furthermore, extensive old inefficient irrigation systems and unlined drainage networks in this region have led to a considerable loss of infiltration to groundwater [50,56]. Zmijewski and Becker [56] estimated the trends in the water balance at the basin scale using the Gravity Recovery and Climate Experiment (GRACE) gravity data, and result showed that water mass lost in the ASB was about 14 km^3/year from 2002 to 2013.

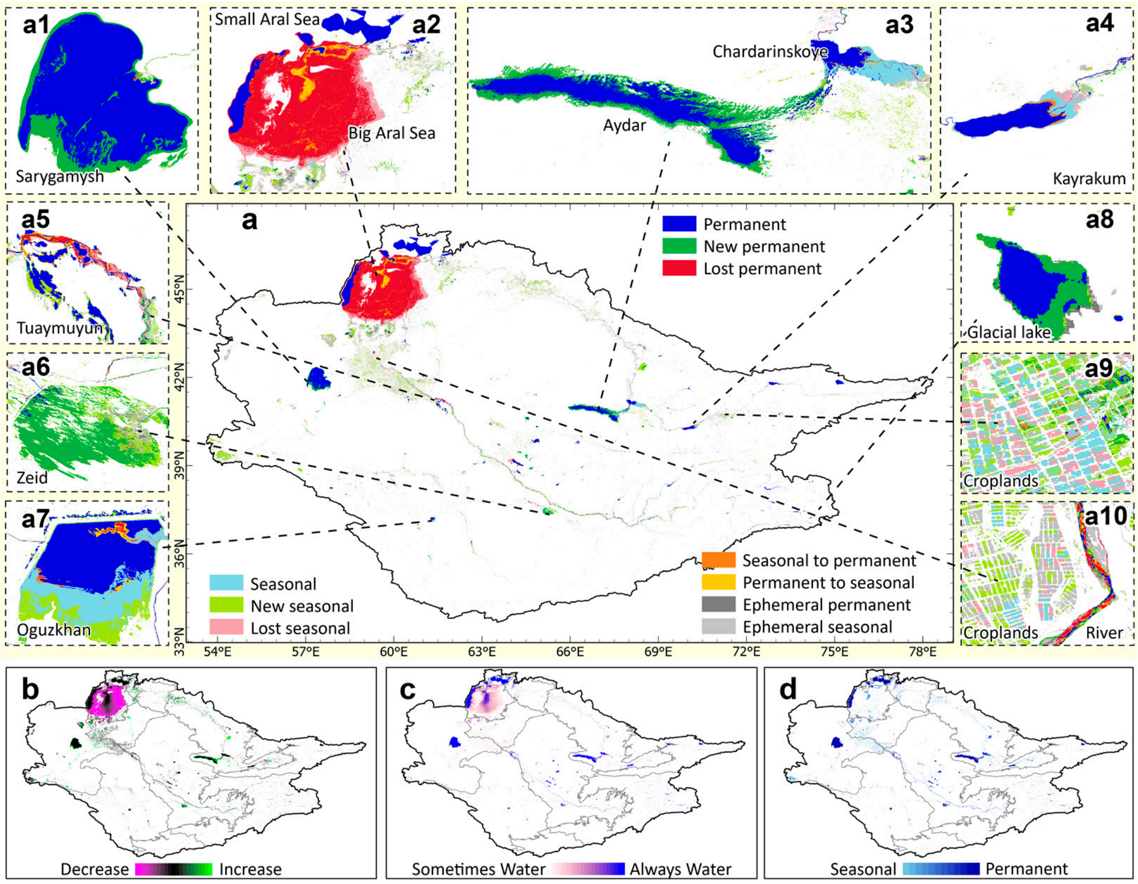

Figure 10. Use of JRC GSW products to produce a series of thematic maps for the ASB. (**a**) Transitions in surface water class during 1984–2020, including the drawing of partial enlargement in 10 typical areas. Of which, a1 to a10 are the local enlarged drawing. (**b**) Intensity of changes in surface water occurrence during 1984–2020. (**c**) Occurrence during 1984–2020. (**d**) Surface water seasonality during 2014–2020. Source from the EC JRC/Google.

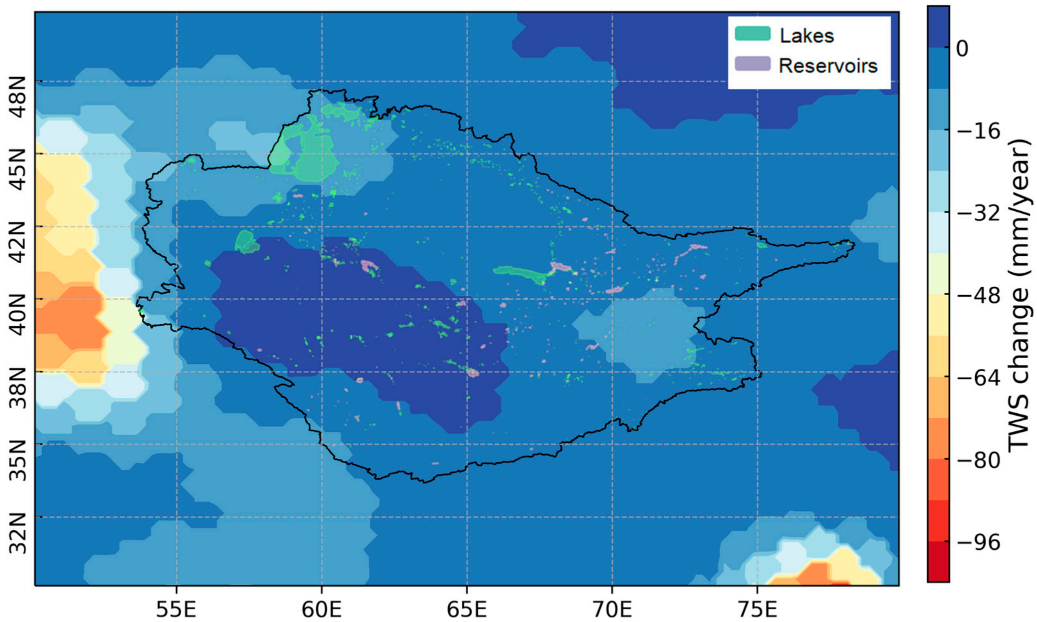

Figure 11. TWS changes in terms of the equivalent water thickness in the ASB from 2003 to 2020, and locations of the lakes and reservoirs explored in this study are shown. Source from the GRACE CSR mascon solution (https://www2.csr.utexas.edu/grace/RL06_mascons.html, accessed on 19 December 2021).

4.4. Comparison of Our Surface Water Inventory with Previous Studies

According to Pekel et al. some new permanent lakes/reservoirs form in the CA while others are lost due to the canal's diversion of the Amu Darya [21]. Additionally, previous studies have respectively pointed out that seasonal water bodies can be created by periodical irrigation [28] and runoff of glacier meltwater [45], but such seasonal water bodies can also disappear due to drought or new dams. Therefore, it is necessary to re-examine the earlier descriptions of surface water in ASB and investigate the distribution of lakes and reservoirs in the region [7].

Previous studies have indicated that the rapid development of agriculture and inefficient drainage in ASB have exacerbated regional discrepancies in surface water resources [61]. This study quantified these regional differences in the surface water of ASB for the first time based on multi-source data. Specifically, permanent water and seasonal water area changes were quantified separately. Moreover, the area of reservoirs, lakes, lakes/reservoirs, and surface water in each region was counted, which has not been carried out in ASB or elsewhere in Central Asia. Existing studies of the lakes in ASB focused mainly on a single lake or some typical lakes; research involving as many lakes as possible is still lacking. To our knowledge, few studies have quantified the lake changes at a whole basin scale. Compared with previous studies, the present surface water inventory has the following advantages. Firstly, it not only describes the time-series characteristics of surface water but also establishes a list of 1559 lakes and 196 reservoirs. Secondly, by extracting the annual area of permanent water and seasonal water during 1992–2020, it clarifies the dynamic process of different water body types in ASB for the first time. Lastly, through a "basin–region–subregion" three-level analysis of the surface water, it captures the inter-regional differences of the water resources in ASB for the first time.

This study provides a detailed and comprehensive investigation of surface water in the ASB and its subregions, and it certifies that the cloud-based GEE method can be used to efficiently explore the surface water area. The present study further raised a framework to identify lakes and reservoirs from the JRC GSW dataset based on multiple open-source data. While the simple and explicit GIS-based framework developed in this study has an advantage in monitoring surface water at a large scale, it does have some limitations. Firstly, this method relies highly on the JRC GSW dataset. Although this dataset is attributed to its relatively higher accuracy of surface water extraction and has been widely used [62], the fine-spatial–temporal monitoring method is still lacking to reflect the subtle variabilities in surface water [63]. Secondly, this framework only focuses on surface water area changes and does not account for variations in the volume of lakes and reservoirs. Water storage is not solely dependent on area, but also on underwater terrain, which can impact the volume of water a lake or reservoir can hold [64]. For example, a large lake may have a low volume if it is very shallow, while a small lake may have a large volume if it is very deep. To provide a more complete understanding of surface water changes in the ASB, future studies could explore lake storage as well, as it is necessary for a better understanding of the role of lakes and reservoirs in large-scale hydrological processes [65].

5. Conclusions

This study investigated the long-term dynamics of surface water in the ASB using the GEE platform. To build a list of water areas for 1559 lakes and 196 reservoirs in ASB from 1992 to 2020, multi-source datasets were integrated, primarily from JRC GSW dataset and supplemented by HydroLAKES databases, Geo-referenced dams databases, and OSM data. The results indicated that from 1992 to 2020, surface water in ASB covered an average total area of 53,675.01 km^2. Of this, 196 reservoirs and 1559 lakes covered an average total area of 3879.08 km^2 and 34,999.61 km^2, respectively. Through a three-level analysis of "basin–region–subregion", three crucial findings were made in this study: (i) The share of permanent water in the surface water of ASB has gradually declined, while the share of seasonal water in the surface water has continued to increase. (ii) The loss of surface water area in ASB occurred mainly in the Aral Sea. In contrast, the total surface water area in the ASB plain area and the ASB mountain area has increased. (iii) The proportion of lakes/reservoirs area in the total surface water area has decreased. Overall, for the water that should have flowed into the Aral Sea to maintain its permanent water, part of it might continue to be permanent water but show up in other regions, while part of it might convert to seasonal water in other regions (especially in the Aral Sea itself and ASB plain area). The availability of water resources in the ASB is under serious pressure from rising temperatures, rapid urbanization, agricultural development, and unreasonable water use. Therefore, a more systematic and comprehensive understanding of surface water changes is of great significance to ensure the safety of water resources in ASB and maintain regional stability.

Author Contributions: Conceptualization, S.H., X.M. and X.C.; methodology, S.H. and X.M.; software, S.H.; validation, S.H. and J.G.; formal analysis, S.H.; investigation, S.H.; resources, H.F.; data curation, S.H.; writing—original draft preparation, S.H.; writing—review and editing, S.H., X.M. and X.C.; visualization, S.H.; supervision, X.C., P.D.M. and T.V.d.V.; project administration, X.C.; funding acquisition, X.C., T.L., A.K. and P.D.M. All authors have read and agreed to the published version of the manuscript.

Funding: This research was funded by the Key Program of National Natural Science Foundation of China (42230708), and the Strategic Priority Research Program of the Chinese Academy of Sciences, Pan-Third Pole Environment Study for a Green Silk Road (Grant No. XDA20060303), and this research was also jointly supported by the K. C. Wong Education Foundation (GJTD-2020-14), the National Natural Science Foundation of China (32071655), and the Chinese Academy of Sciences President's International Fellowship Initiative (PIFI, Grant No. 2017VCA0002). The authors would like to thank the China Scholarships Council for supporting Shuangyan Huang with a grant during her stay at Ghent University, Ghent, Belgium (ICPIT–International Cooperative Program for Innovative Talents, Grant No. 201904910894).

Data Availability Statement: The data presented in this study are available in this article.

Conflicts of Interest: The authors declare no conflict of interest.

References

1. Yu, B.; Cui, B.; Zang, Y.; Wu, C.; Zhao, Z.; Wang, Y. Long-Term Dynamics of Different Surface Water Body Types and Their Possible Driving Factors in China. *Remote Sens.* **2021**, *13*, 1154. [CrossRef]
2. Chen, T.; Song, C.; Ke, L.; Wang, J.; Liu, K.; Wu, Q. Estimating seasonal water budgets in global lakes by using multi-source remote sensing measurements. *J. Hydrol.* **2021**, *593*, 125781. [CrossRef]
3. Palmer, S.C.J.; Kutser, T.; Hunter, P.D. Remote sensing of inland waters: Challenges, progress and future directions. *Remote Sens. Environ.* **2015**, *157*, 1–8. [CrossRef]
4. Donchyts, G.; Baart, F.; Winsemius, H.; Gorelick, N.; Kwadijk, J.; van de Giesen, N. Earth's surface water change over the past 30 years. *Nat. Clim. Change* **2016**, *6*, 810–813. [CrossRef]
5. Micklin, P. Desiccation of the Aral Sea: A Water Management Disaster in the Soviet Union. *Science* **1988**, *241*, 1170–1176. [CrossRef]
6. Wang, Y.; Ma, J.; Xiao, X.; Wang, X.; Dai, S.; Zhao, B. Long-Term Dynamic of Poyang Lake Surface Water: A Mapping Work Based on the Google Earth Engine Cloud Platform. *Remote Sens.* **2019**, *11*, 313. [CrossRef]
7. Li, J.; Sheng, Y. An automated scheme for glacial lake dynamics mapping using Landsat imagery and digital elevation models: A case study in the Himalayas. *Int. J. Remote Sens.* **2012**, *33*, 5194–5213. [CrossRef]
8. Lawford, R.; Strauch, A.; Toll, D.; Fekete, B.; Cripe, D. Earth observations for global water security. *Curr. Opin. Env. Sust.* **2013**, *5*, 633–643. [CrossRef]
9. Tortini, R.; Noujdina, N.; Yeo, S.; Ricko, M.; Lettenmaier, D.P. Satellite-based remote sensing data set of global surface water storage change from 1992 to 2018. *Earth Syst. Sci. Data* **2020**, *12*, 1141–1151. [CrossRef]
10. Donchyts, G.; Schellekens, J.; Winsemius, H.; Eisemann, E.; van de Giesen, N. A 30 m Resolution Surface Water Mask Including Estimation of Positional and Thematic Differences Using Landsat 8, SRTM and OpenStreetMap: A Case Study in the Murray-Darling Basin, Australia. *Remote Sens.* **2016**, *8*, 386. [CrossRef]
11. Avisse, N.; Tilmant, A.; Müller, M.F.; Zhang, H. Monitoring small reservoirs' storage with satellite remote sensing in inaccessible areas. *Hydrol. Earth Syst. Sci.* **2017**, *21*, 6445–6459. [CrossRef]
12. Papa, F.; Crétaux, J.; Grippa, M.; Robert, E.; Trigg, M.; Tshimanga, R.M.; Kitambo, B.; Paris, A.; Carr, A.; Fleischmann, A.S.; et al. Water Resources in Africa under Global Change: Monitoring Surface Waters from Space. *Surv. Geophys.* **2023**, *44*, 43–93. [CrossRef] [PubMed]
13. Lehner, B.; Döll, P. Development and validation of a global database of lakes, reservoirs and wetlands. *J. Hydrol.* **2004**, *296*, 1–22. [CrossRef]
14. Hayes, N.M.; Deemer, B.R.; Corman, J.R.; Razavi, N.R.; Strock, K.E. Key differences between lakes and reservoirs modify climate signals: A case for a new conceptual model. *Limnol. Oceanogr. Lett.* **2017**, *2*, 47–62. [CrossRef]
15. Mulligan, M.; van Soesbergen, A.; Sáenz, L. GOODD, a global dataset of more than 38,000 georeferenced dams. *Sci. Data* **2020**, *7*, 31. [CrossRef] [PubMed]
16. Lehner, B.; Liermann, C.R.; Revenga, C.; Vörösmarty, C.; Fekete, B.; Crouzet, P.; Döll, P.; Endejan, M.; Frenken, K.; Magome, J.; et al. High-resolution mapping of the world's reservoirs and dams for sustainable river-flow management. *Front. Ecol. Environ.* **2011**, *9*, 494–502. [CrossRef]
17. Downing, J.; Prairie, Y.; Cole, J.; Duarte, C.; Tranvik, L.; Striegl, R.; McDowell, W.; Kortelainen, P.; Caraco, N.F.; Melack, J.M.; et al. The Global Abundance and Size Distribution of Lakes, Ponds, and Impoundments. *Limnol. Oceanogr.* **2006**, *51*, 2388–2397. [CrossRef]
18. Leonard, J.; Crouzet, P.; European, E.A. *Lakes and Reservoirs in the EEA Area*; Office for Official Publications of the European Communities: Luxembourg, 1999.
19. Messager, M.L.; Lehner, B.; Grill, G.; Nedeva, I.; Schmitt, O. Estimating the volume and age of water stored in global lakes using a geo-statistical approach. *Nat. Commun.* **2016**, *7*, 13603. [CrossRef] [PubMed]
20. Khandelwal, A.; Karpatne, A.; Ravirathinam, P.; Ghosh, R.; Wei, Z.; Dugan, H.A.; Hanson, P.C.; Kumar, V. ReaLSAT, a global dataset of reservoir and lake surface area variations. *Sci. Data* **2022**, *9*, 356. [CrossRef]
21. Pekel, J.; Cottam, A.; Gorelick, N.; Belward, A.S. High-resolution mapping of global surface water and its long-term changes. *Nature* **2016**, *540*, 418–422. [CrossRef]
22. Huang, Z.; Xu, J.; Zheng, L. Long-Term Change of Lake Water Storage and Its Response to Climate Change for Typical Lakes in Arid Xinjiang, China. *Water* **2023**, *15*, 1444. [CrossRef]
23. Li, Y.; Yang, W.; Li, J.; Zhang, Z.; Meng, L. A Novel Method for Mapping Lake Bottom Topography Using the GSW Dataset and Measured Water Level. *Remote Sens.* **2022**, *14*, 1423. [CrossRef]
24. Van Vliet, J. Direct and indirect loss of natural area from urban expansion. *Nat. Sustain.* **2019**, *2*, 755–763. [CrossRef]
25. Ganguly, S.; Friedl, M.A.; Tan, B.; Zhang, X.; Verma, M. Land surface phenology from MODIS: Characterization of the Collection 5 global land cover dynamics product. *Remote Sens. Environ.* **2010**, *114*, 1805–1816. [CrossRef]
26. Zhang, Y.; Wang, N.; Yang, X.; Mao, Z. The Dynamic Changes of Lake Issyk-Kul from 1958 to 2020 Based on Multi-Source Satellite Data. *Remote Sens.* **2022**, *14*, 1575. [CrossRef]
27. Luo, S.; Song, C.; Liu, K.; Ke, L.; Ma, R. An Effective Low-Cost Remote Sensing Approach to Reconstruct the Long-Term and Dense Time Series of Area and Storage Variations for Large Lakes. *Sensors* **2019**, *19*, 4247. [CrossRef]
28. Conrad, C.; Kaiser, B.O.; Lamers, J.P.A. Quantifying water volumes of small lakes in the inner Aral Sea Basin, Central Asia, and their potential for reaching water and food security. *Environ. Earth Sci.* **2016**, *75*, 952. [CrossRef]

29. Chen, X.; Zuo, H.; Wang, W.; Duan, J.; Chang, M.; Wang, J. Surface water and aerosol spatiotemporal dynamics and influence mechanisms over drylands. *Geosci. Front.* **2023**, *14*, 101524. [CrossRef]
30. Liu, H.; Chen, Y.; Ye, Z.; Li, Y.; Zhang, Q. Recent Lake Area Changes in Central Asia. *Sci. Rep.* **2019**, *9*, 16277. [CrossRef]
31. Klein, I.; Dietz, A.J.; Gessner, U.; Galayeva, A.; Myrzakhmetov, A.; Kuenzer, C. Evaluation of seasonal water body extents in Central Asia over the past 27 years derived from medium-resolution remote sensing data. *Int. J. Appl. Earth Obs.* **2014**, *26*, 335–349. [CrossRef]
32. Zheng, G.; Bao, A.; Li, J.; Zhang, G.; Xie, H.; Guo, H.; Jiang, L.; Chen, T.; Chang, C.; Chen, W. Sustained growth of high mountain lakes in the headwaters of the Syr Darya River, Central Asia. *Glob. Planet Change* **2019**, *176*, 84–99. [CrossRef]
33. Che, X.; Feng, M.; Sun, Q.; Sexton, J.O.; Channan, S.; Liu, J. The Decrease in Lake Numbers and Areas in Central Asia Investigated Using a Landsat-Derived Water Dataset. *Remote Sens.* **2021**, *13*, 1032. [CrossRef]
34. Li, Y.; Niu, Z.; Xu, Z.; Yan, X. Construction of High Spatial-Temporal Water Body Dataset in China Based on Sentinel-1 Archives and GEE. *Remote Sens.* **2020**, *12*, 2413. [CrossRef]
35. Shugar, D.H.; Burr, A.; Haritashya, U.K.; Kargel, J.S.; Watson, C.S.; Kennedy, M.C.; Bevington, A.R.; Betts, R.A.; Harrison, S.; Strattman, K. Rapid worldwide growth of glacial lakes since 1990. *Nat. Clim. Change* **2020**, *10*, 939–945. [CrossRef]
36. Wang, X.; Xiao, X.; Qin, Y.; Dong, J.; Wu, J.; Li, B. Improved maps of surface water bodies, large dams, reservoirs, and lakes in China. *Earth Syst. Sci. Data* **2022**, *14*, 3757–3771. [CrossRef]
37. Zonn, I.S. *The Turkmen Lake Altyn Asyr and Water Resources in Turkmenistan*; Springer: Berlin/Heidelberg, Germany, 2014.
38. Meyer, M.F.; Labou, S.G.; Cramer, A.N.; Brousil, M.R.; Luff, B.T. The global lake area, climate, and population dataset. *Sci. Data* **2020**, *7*, 174. [CrossRef] [PubMed]
39. Klein, I.; Mayr, S.; Gessner, U.; Hirner, A.; Kuenzer, C. Water and hydropower reservoirs: High temporal resolution time series derived from MODIS data to characterize seasonality and variability. *Remote Sens. Environ.* **2021**, *253*, 112207. [CrossRef]
40. Shi, D.; Shi, Y.; Wu, Q. Multidimensional Assessment of Lake Water Ecosystem Services Using Remote Sensing. *Remote Sens.* **2021**, *13*, 3540. [CrossRef]
41. Bratic, G.; Vavassori, A.; Brovelli, M.A. Review of High-Resolution Global Land Cover. *Int. Arch. Photogramm. Remote Sens. Spatial Inf. Sci.* **2021**, *XLIII-B4-2021*, 175–182. [CrossRef]
42. Miles, E.; McCarthy, M.; Dehecq, A.; Kneib, M.; Fugger, S.; Pellicciotti, F. Health and sustainability of glaciers in High Mountain Asia. *Nat Commun.* **2021**, *12*, 2868. [CrossRef]
43. Bhattacharya, A.; Bolch, T.; Mukherjee, K.; King, O.; Menounos, B.; Kapitsa, V.; Neckel, N.; Yang, W.; Yao, T. High Mountain Asian glacier response to climate revealed by multi-temporal satellite observations since the 1960s. *Nat. Commun.* **2021**, *12*, 4311. [CrossRef]
44. Zheng, G.; Allen, S.K.; Bao, A.; Ballesteros-Cánovas, J.A.; Huss, M.; Zhang, G.; Li, J.; Yuan, Y.; Jiang, L.; Yu, T.; et al. Increasing risk of glacial lake outburst floods from future Third Pole deglaciation. *Nat. Clim. Change* **2021**, *11*, 411–417. [CrossRef]
45. Pritchard, H.D. Asia's shrinking glaciers protect large populations from drought stress. *Nature* **2019**, *569*, 649–654. [CrossRef] [PubMed]
46. Hara, S.L.O.; Hannan, T. Irrigation and Water Management in Turkmenistan: Past Systems, Present Problems and Future Scenarios. *Eur. Asia Stud.* **1999**, *51*, 21–41. [CrossRef]
47. Basso, B.; Martinez-Feria, R.A.; Rill, L.; Ritchie, J.T. Contrasting long-term temperature trends reveal minor changes in projected potential evapotranspiration in the US Midwest. *Nat. Commun.* **2021**, *12*, 1476. [CrossRef] [PubMed]
48. Pascolini-Campbell, M.; Reager, J.T.; Chandanpurkar, H.A.; Rodell, M. A 10 per cent increase in global land evapotranspiration from 2003 to 2019. *Nature* **2021**, *593*, 543–547. [CrossRef]
49. Deng, H.; Chen, Y. Influences of recent climate change and human activities on water storage variations in Central Asia. *J. Hydrol.* **2017**, *544*, 46–57. [CrossRef]
50. Conrad, C.; Usman, M.; Morper-Busch, L.; Schönbrodt-Stitt, S. Remote sensing-based assessments of land use, soil and vegetation status, crop production and water use in irrigation systems of the Aral Sea Basin. A review. *Water Secur.* **2020**, *11*, 100078. [CrossRef]
51. Mahindawansha, A.; Külls, C.; Kraft, P.; Breuer, L. Investigating unproductive water losses from irrigated agricultural crops in the humid tropics through analyses of stable isotopes of water. *Hydrol. Earth Syst. Sci.* **2020**, *24*, 3627–3642. [CrossRef]
52. Wang, X.; Chen, Y.; Li, Z.; Fang, G.; Wang, F.; Liu, H. The impact of climate change and human activities on the Aral Sea Basin over the past 50 years. *Atmos. Res.* **2020**, *245*, 105125. [CrossRef]
53. Micklin, P. *Irrigation in the Aral Sea Basin*; Springer: Berlin/Heidelberg, Germany, 2014.
54. Huang, S.; Chen, X.; Chang, C.; Liu, T.; Huang, Y.; Zan, C.; Ma, X.; De Maeyer, P.; Van de Voorde, T. Impacts of climate change and evapotranspiration on shrinkage of Aral Sea. *Sci. Total Environ.* **2022**, *845*, 157203. [CrossRef]
55. Zhan, S.; Song, C.; Wang, J.; Sheng, Y.; Quan, J. A Global Assessment of Terrestrial Evapotranspiration Increase Due to Surface Water Area Change. *Earth's Future* **2019**, *7*, 266–282. [CrossRef]
56. Zmijewski, K.; Becker, R. Estimating the Effects of Anthropogenic Modification on Water Balance in the Aral Sea Watershed Using GRACE: 2003–12. *Earth Interact* **2014**, *18*, 1–16. [CrossRef]
57. Liu, Z.; Huang, Y.; Liu, T.; Li, J.; Xing, W.; Akmalov, S.; Peng, J.; Pan, X.; Guo, C.; Duan, Y. Water Balance Analysis Based on a Quantitative Evapotranspiration Inversion in the Nukus Irrigation Area, Lower Amu River Basin. *Remote Sens.* **2020**, *12*, 2317. [CrossRef]

58. Water Resources of the Aral Sea Basin. Available online: http://www.cawater-info.net/aral/water_e.htm (accessed on 23 April 2023).
59. Water Management Situation in the Aral Sea Basin. Available online: http://www.cawater-info.net/yearbook/2020/02_yearbook2020_en.htm (accessed on 23 April 2023).
60. Waltham, T.; Sholji, I. The demise of the Aral Sea—An environmental disaster. *Geol. Today* **2001**, *17*, 218–228. [CrossRef]
61. Jiang, L.; Jiapaer, G.; Bao, A.; Yuan, Y.; Zheng, G.; Guo, H.; Yu, T.; De Maeyer, P. The effects of water stress on croplands in the Aral Sea basin. *J. Clean Prod.* **2020**, *254*, 120114. [CrossRef]
62. Tang, H.; Lu, S.; Ali Baig, M.H.; Li, M.; Fang, C.; Wang, Y. Large-Scale Surface Water Mapping Based on Landsat and Sentinel-1 Images. *Water* **2022**, *14*, 1454. [CrossRef]
63. Yang, X.; Qin, Q.; Yésou, H.; Ledauphin, T.; Koehl, M.; Grussenmeyer, P.; Zhu, Z. Monthly estimation of the surface water extent in France at a 10-m resolution using Sentinel-2 data. *Remote Sens. Environ.* **2020**, *244*, 111803. [CrossRef]
64. Feng, Y.; Zhang, H.; Tao, S.; Ao, Z.; Song, C.; Chave, J.; Le Toan, T.; Xue, B.; Zhu, J.; Pan, J.; et al. Decadal Lake Volume Changes (2003–2020) and Driving Forces at a Global Scale. *Remote Sens.* **2022**, *14*, 1032. [CrossRef]
65. Busker, T.; de Roo, A.; Gelati, E.; Schwatke, C.; Adamovic, M.; Bisselink, B.; Pekel, J.; Cottam, A. A global lake and reservoir volume analysis using a surface water dataset and satellite altimetry. *Hydrol. Earth Syst. Sc.* **2019**, *23*, 669–690. [CrossRef]